Lattice Boltzmann simulation of chemical dissolution in porous media

Qinjun Kang
Los Alamos National Laboratory, Los Alamos, New Mexico 87545
and The Johns Hopkins University, Baltimore, Maryland 21218

Dongxiao Zhang
Los Alamos National Laboratory, Los Alamos, New Mexico 87545

Shiyi Chen
The Johns Hopkins University, Baltimore, Maryland 21218
and Peking University, Beijing, China

Xiaoyi He
Los Alamos National Laboratory, Los Alamos, New Mexico 87545

(Received 20 May 2001; revised manuscript received 27 August 2001; published 7 March 2002)

In this paper, we develop a lattice Boltzmann model for simulating the transport and reaction of fluids in porous media. To simulate such a system, we account for the interaction of forced convection, molecular diffusion, and surface reaction. The problem is complicated by the evolution of the porous media geometry due to chemical reactions, which may significantly and continuously modify the hydrologic properties of the media. The particular application that motivates the present study is acid stimulation, a common technique used to increase production from petroleum reservoirs. This technique involves the injection of acid (e.g., hydrochloric acid, HCl, acetic acid, HAc) into the formation to dissolve minerals comprising the rock. As acid is injected, highly conductive channels or ''wormholes'' may be formed. The dissolution of carbonate rocks in 0.5*M* HCl and 0.5*M* HAc is simulated with the lattice Boltzmann model developed in this study. The dependence of dissolution process and the geometry of the final wormhole pattern on the acid type and the injection rate is studied. The results agree qualitatively with the experimental and theoretical analyses of others and substantiate the previous finding that there exists an optimal injection rate at which the wormhole is formed as well as the number of pore volumes of the injected fluid to break through is minimized. This study also confirms the experimentally observed phenomenon that the optimal injection rate decreases and the corresponding minimized number of pore volumes to break through increases as the acid is changed from HCl to HAc. Simulations suggest that the proposed lattice Boltzmann model may serve as an alternative reliable quantitative approach to study chemical dissolution in porous media.

DOI: 10.1103/PhysRevE.65.036318 PACS number(s): 47.55.Mh

I. INTRODUCTION

The transport and reaction of fluids in porous media is a topic of great importance for a wide range of scientific problems, such as stimulation of petroleum reservoirs, environmental contaminant transport, mineral mining, geologic sequestration of carbon dioxide, chemical weathering, diagenesis, concrete degradation, and bioremediation. These problems usually involve multiple processes: the convection of fluid, which may carry reactants as well as products: the diffusion of reactants and products to and from the solid-liquid interface; chemical reaction at the solid-liquid interface. These problems are further complicated by the evolution of the porous media geometry due to chemical reactions, which may significantly and continuously modify the hydrologic properties of the media. The particular application that motivates the present study is acid stimulation, a common technique used to increase production from petroleum reservoirs. This technique involves the injection of acid (e.g., hydrochloric acid, HCl, acetic acid, HAc) into the formation to dissolve minerals comprising the rock. As acid is injected, highly conductive channels or ''wormholes'' are usually formed. Wormhole formation is the dominant mechanism by which the fluid conductivity is increased. It is an effective means of stimulating the formation for oil or gas to flow more readily.

Due to its importance, a solution to the problem of coupled transport and reaction in porous media has been attempted by various approaches. At a macroscopic (i.e., Darcy) scale, it has been studied with a set of partial differential equations [1–9]. Under the condition that the dissolution process does not increase the porosity dramatically, fingering, the formation of channels wherein the dissolution is not complete, has been modeled using the Darcy equation in both homogeneous and heterogeneous porous media. It has been shown that an increase of the fluid advection rate leads to narrower and longer fingers [3,4]. Numerical simulations of wormholing, the formation of channels wherein the matrix is completely removed through dissolution, have been achieved using Brinkman's equation. Simulations in various media show that the size of channels is determined by the system's fluid/rock chemical and hydrodynamic characteristics [8,9]. At a microscopic scale, with an experiment performed on plaster, Daccord [10] observed the formation of a

highly branched wormhole network. Wells, Janecky, and Travis [11] used a lattice gas automata (LGA) to simulate the coupled solute transport and chemical reaction at mineral surfaces and in pore networks. Janecky *et al.* [12] applied a similar method for simulating geochemical systems. With an experimental study and lattice Boltzmann simulations, Kelemen *et al.* [13] demonstrated the phenomenon of channel growth in the presence of and in the absence of an initial solution front where there is a gradient in the solubility of the solid matrix. Bekri, Thovert, and Adler [14] applied numerical schemes based on random walks as well as a finite difference formulation to studying the dissolution of porous media in the quasisteady limit where the geometrical changes are very slow. Under the same conditions, they also studied the deposition and/or dissolution of a single solute in a single fracture by means of an efficient finite-difference scheme [15]. Also, the dissolution phenomenon has been investigated with analog network simulations [16,17]. The simulation results were in qualitative agreement with acidizing experiments. In this paper, we present a lattice Boltzmann model for simulating the coupled flow and chemical reaction in porous media. We aim to systematically consider the dynamic process of convection, diffusion, and reaction as well as the complex geometry of natural porous media and its evolution due to the chemical reaction.

Unlike conventional numerical schemes based on discretizations of macroscopic continuum equations, the lattice Boltzmann method (LBM) is based on microscopic models and mesoscopic kinetic equations [18]. This feature gives LBM the advantage of studying nonequilibrium dynamics, especially in fluid flow applications involving interfacial dynamics and complex boundaries (geometries). Using the ensemble averaged distribution function as the primary variable instead of tracking individual molecules allows LBM to be carried out with less computational cost than those methods based on molecular dynamics.

Since its appearance, the LBM has been successfully applied to studying a variety of flow and transport phenomena such as flow in porous media [19–22], turbulence [23], multiphase and multicomponent flows [24–27], particles suspended in fluids [28], and heat transfer [29–31]. Compared to other applications, there are relatively few studies using the LBM to study chemical reactions. Most studies on diffusion-reaction problems made use of LGA. However, as indicated in a review paper by Chen *et al.* [32], it is very difficult to incorporate fluid convection in the LGA diffusion-reaction models. In addition, the intrinsic noise in the LGA prevents these models from becoming practical numerical simulation tools for engineering applications. Among the relatively few LGA and LBM chemical reaction models, most of them deal with the chemical reactions in bulk fluids [33,34]; we are, however, particularly interested in the chemical reaction on solid surfaces. The relevant studies are those by Wells, Janecky, and Travis [11], Janecky *et al.* [12], Kelemen *et al.* [13], and He, Li, and Goldstein [35]. In the first two studies, surface reactions involving dissolution and precipitation were modeled with LGA by allowing wall nodes to serve as sources or sinks for a mass of a dissolved component. The mass transfer between fluid and solid surface depends on the disequilibrium between the fluid and mineral. Keleman *et al.* [13] implemented a dissolution concept similar to the above-mentioned one in their lattice Boltzmann model. He, Li, and Goldstein [35] explicitly incorporated the reaction kinetics into the LBM model. This was done by coupling the surface reaction with the diffusion between the wall and the bulk fluid. The present paper extends the latter approach to flow and transport in arbitrary geometries and with locally unsteady state reactions, which are closer to the process of acidization of carbonate reservoirs.

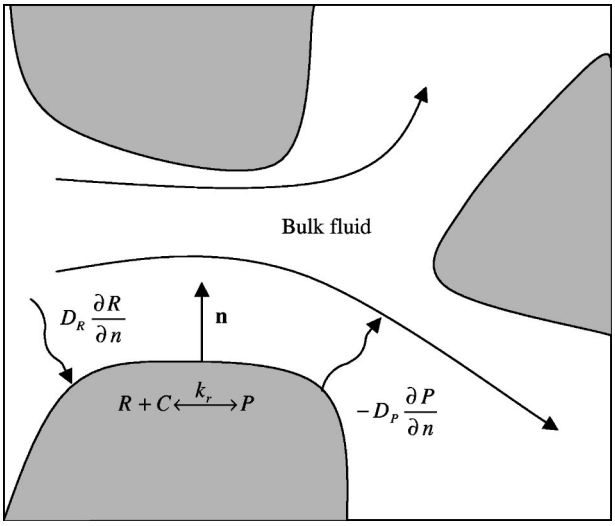

FIG. 1. Schematic illustration of pore-scale processes: convection and diffusion of reactant and product, and reversible chemical reaction on the surface.

The rest of the paper is organized as follows. Section II describes a comprehensive dissolution model proposed by Fredd and Fogler [17]. Section III describes the lattice Boltzmann scheme for simulating a convection-diffusion system with surface chemical reaction in arbitrary geometries. Section IV presents several simulations of acidization of carbonate reservoirs to validate the proposed LBM scheme while Sec. V concludes the paper.

II. A COMPREHENSIVE DISSOLUTION MODEL

In the paper of Fredd and Fogler [17], the overall carbonate dissolution mechanism has been modeled as three sequential processes. These processes include the mass transfer of reactants to the carbonate surface, the reversible surface reactions, and the mass transfer of products away from the carbonate surface. To simplify the illustration of this development, the surface reactions have been generalized as

$$(\text{Reactants}) + \text{CaCO}_3 \rightleftharpoons (\text{Products}), \tag{1}$$

which can be simplified as

$$R + C \rightleftharpoons P. \tag{2}$$

Both reactant R and product P are soluble in the bulk fluid, and reactant C is bound at the solid surface (see Fig. 1).

Assuming that the dissolution occurs by a first-order heterogeneous chemical reaction, the rate of dissolution (r_D) is then given by

$$r_D = k_r(R - P/K_{\mathrm{eq}}), \tag{3}$$

where k_r is the effective forward reaction rate constant, K_{eq} is the effective equilibrium constant, and R and P are the reactant and product concentrations at the solid-liquid interface, respectively. The effective reaction rate and equilibrium constants for this generalized reaction depend on which reaction mechanism is dominating the dissolution and, therefore, depend on the pH and the type of species present.

Although the above model is based on the dissolution of calcite, it is a general form applicable to other reaction systems when k_r and K_{eq} can be determined.

III. LATTICE BOLTZMANN MODEL FOR SURFACE REACTION IN FLOW SYSTEMS

A. Evolution equations

In this study, we assume that the solute concentrations are sufficiently low not to influence the solvent flow. The solute transport in such a system can be described by the following lattice Boltzmann equation:

$$g_\alpha^s(\mathbf{x}+\mathbf{e}_\alpha\delta_t, t+\delta_t) - g_\alpha^s(\mathbf{x},t) = -\frac{g_\alpha^s(\mathbf{x},t) - g_\alpha^{s,\mathrm{eq}}(C^s,\mathbf{u})}{\tau_s} + \omega_\alpha q^s, \tag{4}$$

where g_α^s is the distribution function of the concentration of the sth solute; τ_s is the relaxation time; and q^s is the source term associated with chemical reaction in bulk fluids. The superscript stands for the sth species. $g_\alpha^{s,\mathrm{eq}}$ is the corresponding equilibrium distribution:

$$g_\alpha^{s,\mathrm{eq}}(C^s,\mathbf{u}) = \omega_\alpha C^s\left[1 + \frac{\mathbf{e}_\alpha\cdot\mathbf{u}}{\mathcal{R}T} + \frac{(\mathbf{e}_\alpha\cdot\mathbf{u})^2}{2(\mathcal{R}T)^2} - \frac{\mathbf{u}^2}{2\mathcal{R}T}\right], \tag{5}$$

where $\mathcal{R}$ is the gas constant, $\mathbf{u}$ and T are the velocity and temperature of the solvent fluid, respectively, and C^s is the concentration of the sth solute. $\mathbf{e}_\alpha$'s are the discrete velocities and ω_α's are the associated weight coefficients. For the 2D (two-dimensional) nine-speed LBM model, we have $\mathcal{R}T = 1/3$, and

$$e_\alpha = \begin{cases} 0, & \alpha = 0, \\ \left(\cos\dfrac{(\alpha-1)\pi}{2}, \quad \sin\dfrac{(\alpha-1)\pi}{2}\right), & \alpha = 1-4, \\ \sqrt{2}\left(\cos\left[\dfrac{(\alpha-5)\pi}{2} + \dfrac{\pi}{4}\right], \quad \sin\left[\dfrac{(\alpha-5)\pi}{2} + \dfrac{\pi}{4}\right]\right), & \alpha = 5-8. \end{cases} \tag{6}$$

The corresponding weight coefficients are $\omega_0 = 4/9$, $\omega_\alpha = 1/9$ for $\alpha = 1,2,3,4$, and $\omega_\alpha = 1/36$ for $\alpha = 5,6,7,8$. The concentration of the sth species is calculated using

$$C^s = \sum_\alpha g_\alpha^s. \tag{7}$$

Using the Chapman-Enskog expansion technique, the above lattice Boltzmann equation can be proven to recover the following convection-diffusion-reaction equation [34]:

$$\frac{\partial C^s}{\partial t} + (\mathbf{u}\cdot\nabla)C^s = \nabla\cdot(D_s\nabla C^s) + q^s, \tag{8}$$

where the diffusion coefficient of the sth component D_s is related to the corresponding relaxation time via $D_s = (\tau_s - 0.5)\mathcal{R}T$.

Since we have assumed that the solute concentrations are sufficiently low, the solvent fluid can be simulated using the following lattice Boltzmann equation:

$$f_\alpha(\mathbf{x}+\mathbf{e}_\alpha\delta_t, t+\delta_t) - f_\alpha(\mathbf{x},t) = -\frac{f_\alpha(\mathbf{x},t) - f_\alpha^{\mathrm{eq}}(\rho,\mathbf{u})}{\tau}, \tag{9}$$

where f_α is the distribution function of the solvent, τ is the relaxation time relating to the kinematic viscosity by $\nu = (\tau - 0.5)\mathcal{R}T$; and f_α^{eq} is the equilibrium distribution of f_α:

$$f_\alpha^{\mathrm{eq}}(\rho,\mathbf{u}) = \omega_\alpha\rho\left[1 + \frac{\mathbf{e}_\alpha\cdot\mathbf{u}}{\mathcal{R}T} + \frac{(\mathbf{e}_\alpha\cdot\mathbf{u})^2}{2(\mathcal{R}T)^2} - \frac{\mathbf{u}^2}{2\mathcal{R}T}\right]. \tag{10}$$

The density and velocity of the bulk fluid are calculated using

$$\rho = \sum_\alpha f_\alpha, \tag{11}$$

$$\rho\mathbf{u} = \sum_\alpha \mathbf{e}_\alpha f_\alpha. \tag{12}$$

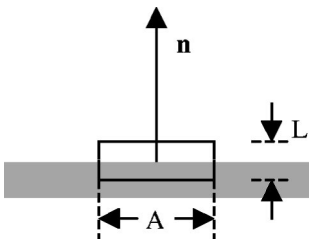

FIG. 2. A typical control volume on the wall.

It is well known that, using the Chapman-Enskog expansion, the above lattice Boltzmann equation (9) recovers the correct continuity and momentum equations at the Navier-Stokes level,

$$\frac{\partial \rho}{\partial t} + \nabla \cdot (\rho \mathbf{u}) = 0, \tag{13}$$

$$\rho \left[\frac{\partial \mathbf{u}}{\partial t} + (\mathbf{u} \cdot \nabla)\mathbf{u} \right] = -\nabla p + \nabla \cdot [\rho \nu (\nabla \mathbf{u} + \mathbf{u} \nabla)], \tag{14}$$

where $p = \rho \mathcal{R} T$ is the fluid pressure.

In the simulation, the convection-diffusion-reaction equation (8) is coupled with the flow equation (14) through the velocity field **u**; the flow field is being continuously modified because of the evolution of pore geometry due to chemical dissolutions, which are strongly dependent on the transport and reaction of the fluids.

B. Boundary conditions

From the consideration of mass conservation of product P within a control volume on the boundary (see Fig. 2),

$$\frac{\partial}{\partial t} \int P' dV = \int \left(r_D + D_P \frac{\partial P}{\partial n} \right) dA, \tag{15}$$

where D_P is diffusivity of P, P' is the density of the product in the control volume, which has the dimension of concentration. Suppose all quantities are uniform on A, then

$$\frac{\partial}{\partial t} \int P' A dl = \left(r_D + D_P \frac{\partial P}{\partial n} \right) A, \tag{16}$$

or

$$\frac{\partial}{\partial t} \int P' dl = r_D + D_P \frac{\partial P}{\partial n}, \tag{17}$$

$$\frac{\partial}{\partial t} (\overline{P'} L) = r_D + D_P \frac{\partial P}{\partial n}, \tag{18}$$

where $\overline{P'}$ is the average of P' over the depth, which is generally not equal to the concentration at the solid-liquid interface of the boundary layer. They may be related using a characteristic length L' of the boundary layer, on the basis of $PL' = \overline{P'L}$. Then

$$\frac{\partial}{\partial t} (PL') = r_D + D_P \frac{\partial P}{\partial n}, \tag{19}$$

$$L' \frac{\partial P}{\partial t} = r_D + D_P \frac{\partial P}{\partial n}, \tag{20}$$

where the change of L' with time is assumed negligible. Similarly, for the reactant solute concentration R

$$L' \frac{\partial R}{\partial t} = -r_D + D_R \frac{\partial R}{\partial n}, \tag{21}$$

where D_R is the diffusivity of R. When the boundary layer characteristic length $L' \to 0$, the local reaction and diffusion processes become steady state, namely, the dissolution rate is equal to the mass transfer rate of solute reactant toward the solid interface and that of product away from there. This locally steady state assumption has been made by Fredd and Fogler [17]. In this paper, however, we consider the more general case described by Eqs. (20)–(21).

If we discretize the time derivative terms with the first-order forward difference scheme, after reorganizing them, we obtain

$$D_R \frac{\partial R}{\partial n} = h_R (R - R_\infty), \tag{22}$$

$$D_P \frac{\partial P}{\partial n} = h_P (P - P_\infty), \tag{23}$$

where

$$h_R = k_r + \frac{L'}{\Delta t}, \tag{24}$$

$$R_\infty = \frac{\dfrac{k_r}{K_{\mathrm{eq}}} P_0 + R_0 \dfrac{L'}{\Delta t}}{h_R}, \tag{25}$$

$$h_P = \frac{k_r}{K_{\mathrm{eq}}} + \frac{L'}{\Delta t}, \tag{26}$$

$$P_\infty = \frac{k_r R_0 + P_0 \dfrac{L'}{\Delta t}}{h_P}, \tag{27}$$

where R_0, P_0 are concentrations of the soluble reactant and product at the previous time step, respectively. Unlike conventional diffusion problems, R_∞ and P_∞ both vary with time in our case because of the surface reaction.

The above formulations describe a boundary condition for surface reaction at the macroscopic level. To implement this into an LBM model, we have to formulate a boundary condition for the distribution functions. For this purpose, we utilize an approach similar to the thermal LBM model proposed by He, Chen, and Doolen [31]. This approach is based on the observation that, at a stationary wall, the nonequilibrium portion of the distribution function is proportional to

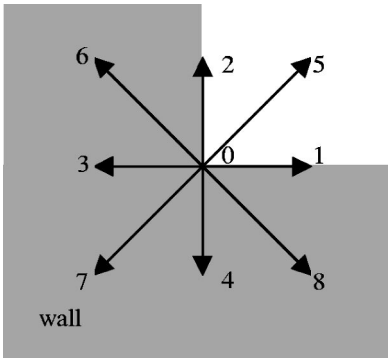

FIG. 3. A wall node at the left bottom corner.

the dot product of its microscopic velocity and the concentration gradient. Consequently, the nonequilibrium portion in opposite directions takes opposite signs. Taking a wall node in the left bottom corner as an example (see Fig. 3), the above consideration leads to the following boundary conditions:

$$C^s = \frac{g_7^s + \beta^s C_\infty^s}{\beta^s + \omega_7}, \tag{28}$$

which is applicable for both reactant R and product P with $C^1 = R$, $C^2 = P$, $C_\infty^1 = R_\infty$, $C_\infty^2 = P_\infty$, $\beta^1 = 1/32(h_R/D_R)$, and $\beta^2 = 1/32(h_P/D_P)$. On the basis of C^s and $\mathbf{u}$, $g_\alpha^{s,\mathrm{eq}}$ can be calculated from Eq. (5). Then the distribution functions can be calculated:

$$g_1^s = g_1^{s,\mathrm{eq}} + g_3^{s,\mathrm{eq}} - g_3^s, \tag{29}$$

$$g_2^s = g_2^{s,\mathrm{eq}} + g_4^{s,\mathrm{eq}} - g_4^s, \tag{30}$$

$$g_5^s = g_5^{s,\mathrm{eq}} + g_7^{s,\mathrm{eq}} - g_7^s, \tag{31}$$

and

$$g_6^s = g_6^{s,\mathrm{eq}} + \frac{g_3^s - g_4^s}{4\sqrt{2}}, \tag{32}$$

$$g_8^s = g_8^{s,\mathrm{eq}} - \frac{g_3^s - g_4^s}{4\sqrt{2}}. \tag{33}$$

IV. SIMULATION RESULTS AND DISCUSSION

The two-dimensional geometry used in our simulations is a cross-section of a pore geometry set of $180\times217\times217$ voxels obtained with computed microtomography [22]. The resolution of the original set is 2.7 μm in each direction, and the sample size is $0.486\times0.586\times0.586$ mm. For the purpose of illustration, the material here is considered to be limestone. In the lattice Boltzmann simulation, the 2D domain is discretized into 90×108 nodes with lattice unit length being 5.4 μm. The acids used in the simulations are 0.5M HAc and 0.5M HCl, respectively. Their parameters are given in Table I [17]. In the simulation domain, we add a few arrays of void space at both the left and right boundaries. At the left inlet boundary, uniform velocity is specified: at the right outlet boundary, the density (pressure) is fixed; the top and bottom boundaries are stationary walls, which do not participate in the chemical reaction. In this study, we neglect the chemical reaction in the bulk fluid.

TABLE I. Parameters used in the simulations.

Type of acid	D_R (cm^2/s)	D_p (cm^2/s)	k_r (cm/s)	K_{eq}
0.5M HCl	3.6×10^{-5}	2×10^{-5}	2×10^{-1}	1×10^{10}
0.5M HAc	1.1×10^{-5}	8×10^{-6}	5×10^{-3}	1.6×10^{-1}

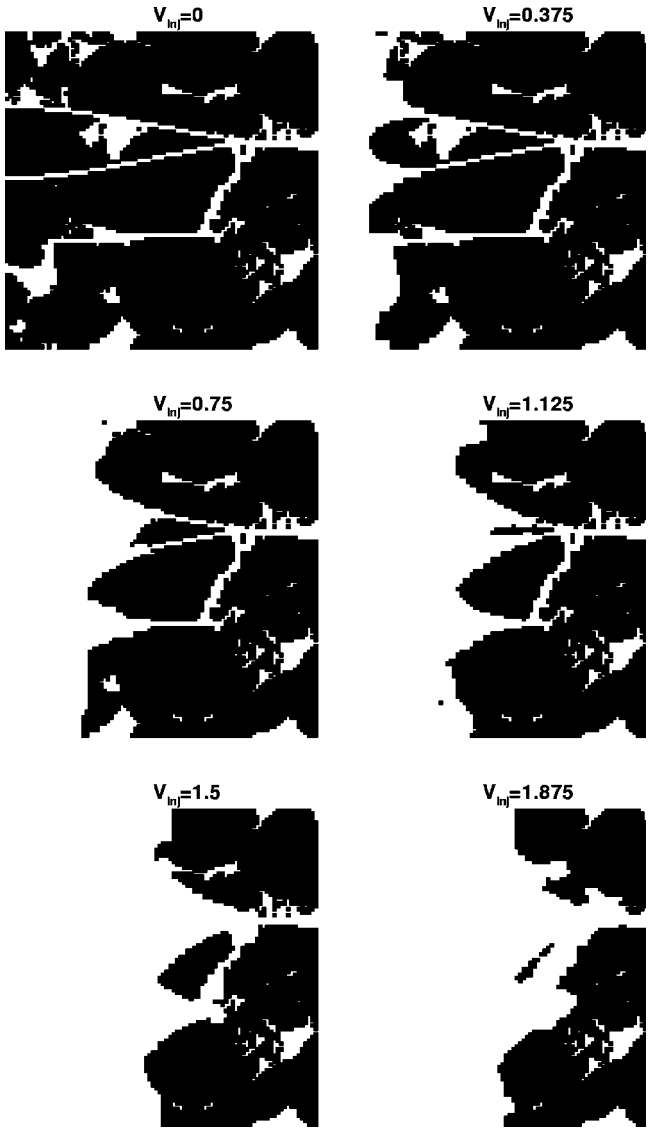

FIG. 4. Evolution of pore geometry due to dissolution by 0.5M HCl injected with the rate of $Q = 0.0215$ cm^3/min at the left-hand side. V_{inj} stands for the volume of injected acid in terms of the initial pore volume of the medium.

Figure 4 shows the dissolution process with HCl injected from the left inlet at a very low flow rate ($Q = 0.0215$ cm^3/min). At this flow rate, the reactant is consumed on the inlet flow face of the material, resulting in the complete dissolution of the solids starting from the inlet flow

TABLE II. V_{BT} and P_{BT} at different injection rates of HCl.

Injection rate (cm^3/min)	0.0215	0.129	0.43
V_{BT}	2.15	1.42	4.1
P_{BT}	3.1	2.44	2.35

face. In other words, there is a dissolution front that moves from left to right. Solids on this front are totally dissolved. This is called face dissolution. In this case, there are no dominant channels formed, and the corresponding permeability increase is not significant because a significant part of the medium is unaffected by the dissolution. In the last picture, the number of pore volumes (V_{inj}) has not reached the value to break through even though more than half of the medium has been removed. The number of pore volumes (V_{inj}) is defined as the ratio of the volume of fluid injected to the volume of the pore space in the original medium; the

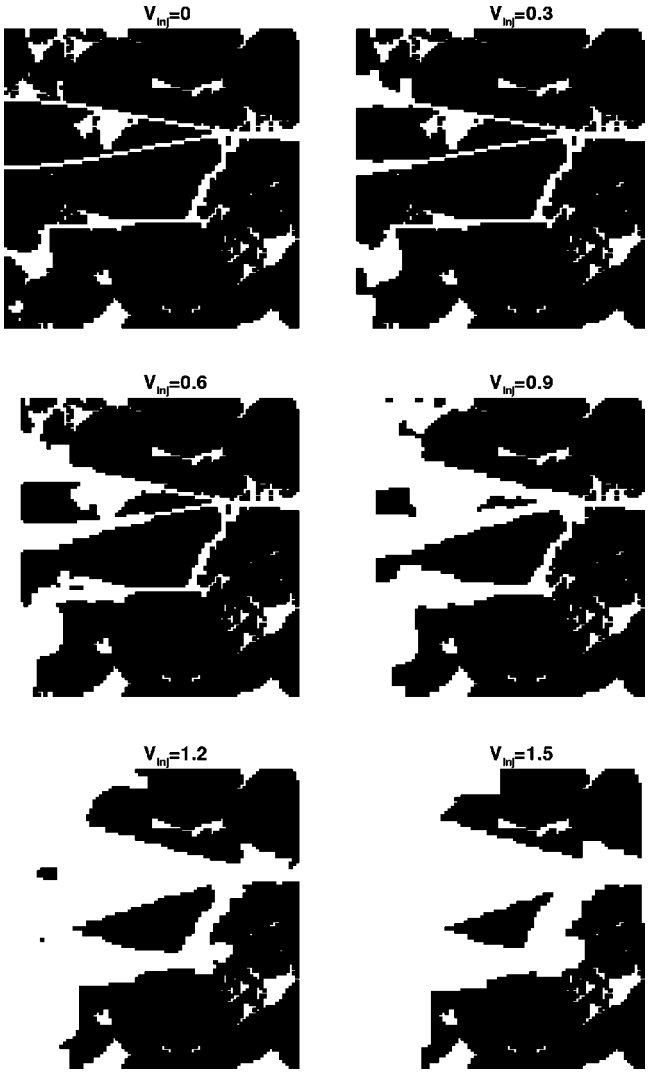

FIG. 5. Evolution of pore geometry due to dissolution by 0.5*M* HCl injected with the rate of $Q=0.129\ cm^3$/min at the left-hand side. V_{inj} stands for the volume of injected acid in terms of the initial pore volume of the medium.

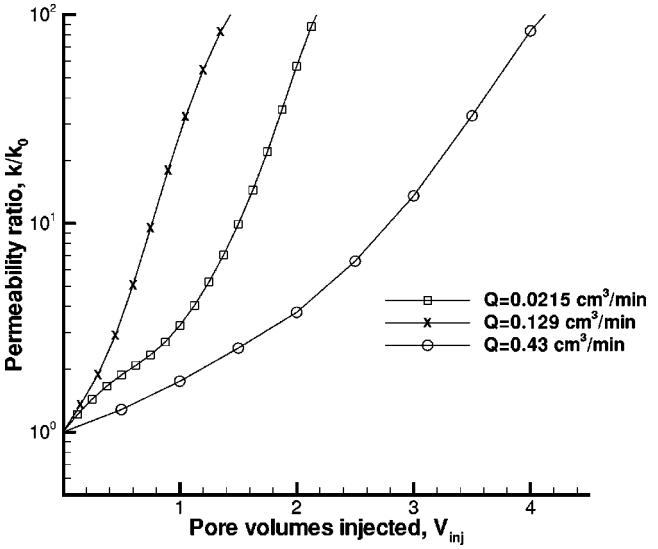

FIG. 6. Enhancement of permeability due to acid dissolution for three injection rates of 0.5*M* HCl. It suggests that there exists an optimal injection rate (in this case, $Q=0.129\ cm^3$/min) at which permeability enhancement is the fastest.

breakthrough point is defined as the point at which the ratio between the permeability values after (k) and before (k_0) acid injection reaches 100 (see Table II for details). At a higher injection rate ($Q=0.129\ cm^3$/min), the reactant can penetrate into the porous matrix and enlarge flow channels. A significant amount of reactant is consumed on the walls of the flow channels. Unconsumed reactant reaches the tip of the evolving flow channels and reacts with the solids there. This consumption propagates the dissolution channels and eventually results in the formation of dominant wormhole channels (see Fig. 5). The formation of wormholes provides significant permeability increase and requires a minimum pore volumes of fluid to break through (or percolate) the rock matrix. In the last one of this group of pictures, the number of pore volumes has exceeded the number of pore volumes at breakthrough (V_{BT}), although more than half of the media remains. As the injection rate goes higher ($Q=0.43\ cm^3$/min), the flow channels become more highly branched or ramified as fluid is forced into smaller pores. Moreover, a significant part of the reactant flows away from the rock matrix before it reacts with it, resulting in the increase of fluid needed to break through.

It is seen from Fig. 6 and Table II that at flow rates $Q=0.0215\ cm^3$/min, $Q=0.129\ cm^3$/min, and $Q=0.43\ cm^3$/min the numbers of pore volumes to break through (V_{BT}) are 2.15, 1.42, and 4.1, respectively. Also from Table II, we find that the porosity response is more sensitive at a low injection rate. At the three flow rates from low to high, the porosity

TABLE III. V_{BT} and P_{BT} at different injection rates of HAc.

Injection rate (cm^3/min)	0.0086	0.043	0.215
V_{BT}	8.9	4.16	16.9
P_{BT}	3.15	2.3	2.2

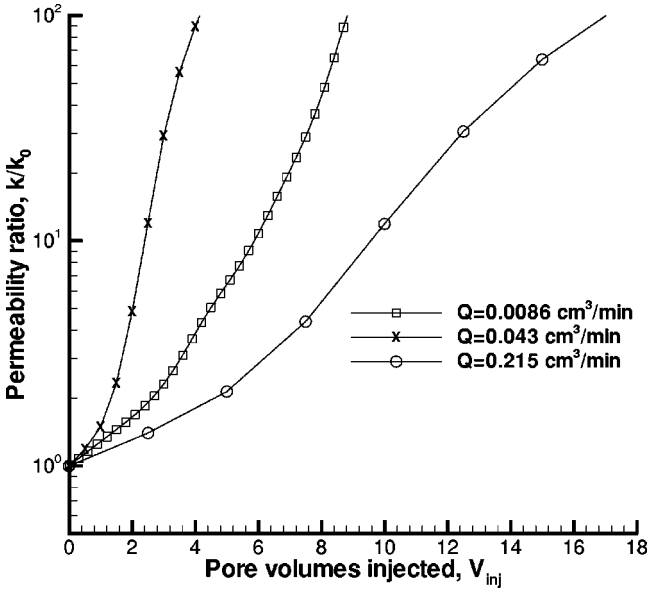

FIG. 7. Enhancement of permeability due to acid dissolution for three injection rates of 0.5*M* HAc. It suggests that there exists an optimal injection rate (in this case, $Q=0.043\ \mathrm{cm}^3/\mathrm{min}$) at which permeability enhancement is the fastest.

ratio at breakthrough point (P_{BT}) are 3.1, 2.44, and 2.35, respectively. This is reasonable because at a low injection rate, the liquid reactant has enough time to fully react with the rock matrix before it is taken away by the fluid. Although the face dissolution does not increase the permeability significantly, it does increase the porosity.

Similar phenomena are observed in the simulation of 0.5*M* HAc. Face dissolution is seen at a low injection rate and the formation of dominant wormhole channels is observed with an increased injection rate. There also exists an optimal injection rate at which the number of pore volumes to break through is minimized (see Table III and Fig. 7). The porosity ratio at breakthrough also increases as the injection rate decreases (Table III). The number of pore volumes to break through at the optimal injection rate is greater than that for HCl. This is understandable because the forward reaction of HAc with limestone is slower than that of HCl of the same concentration with limestone, and is more reversible as well. Thus, naturally, the minimal number of pore volumes to break through is greater and the corresponding injection rate is smaller. Previous experiments have observed this but previous 2D network simulations failed to predict it [17].

V. CONCLUSIONS

We have developed a lattice Boltzmann model for simulation of the transport and reaction of fluids in porous media. We used the developed model to simulate the acid stimulation process in a limstone reservoir. The simulation results of dissolution of limestone in 0.5*M* HCl and 0.5*M* HAc showed qualitative agreements with experimental and theoretical investigations [17]. Our results verified the experimental observation that there exists an optimal injection rate at which the wormhole is formed as well as the number of pore volumes to break through is minimized. The lattice Boltzmann model also successfully confirmed the dependence of the optimal injection rate and the minimized number of pore volumes to break through on the type of acids while a previous network modeling approach failed [17].

Our simulations suggest that the LB model may be a reliable numerical technique to study chemical dissolution in porous media. The present paper is only the first step toward this topic. The coupled transport and reaction is a highly nonlinear and dynamic system influenced by a number of key parameters such as acid concentration, acid injection rate, chemical reaction rate, characteristic length scale of the porous media, and diffusion constant. Investigating the effects of these parameters and finding out the nondimensional control parameters are topics of our future work.

[1] J. Chadam, D. Hoff, E. Merino, P. Ortoleva, and A. Sen, IMA J. Appl. Math. **36**, 207 (1986).
[2] P. Ortoleva, J. Chadam, E. Merino, and A. Sen, Am. J. Sci. **287**, 1008 (1987).
[3] W. Chen and P. Ortoleva, Earth-Sci. Rev. **29**, 183 (1990).
[4] C. I. Steefel and A. C. Lasaga, Chem. Modeling Aqueous Syst. **II**, 212 (1990).
[5] C. I. Steefel and A. C. Lasaga, Am. J. Sci. **294**, 529 (1994).
[6] E. Aharonov, J. Whitehead, P. B. Kelemen, and M. Spiegelman, J. Geophys. Res., [Solid Earth] **100**, 20 433 (1995).
[7] E. Aharonov, M. Spiegelman, and P. B. Kelemen, J. Geophys. Res., [Solid Earth] **102**, 14 821 (1997).
[8] X. Liu, A. Ormond, K. Bartko, Y. Li, and P. Ortoleva, J. Pet. Sci. Eng. **17**, 181 (1997).
[9] A. Ormond and P. Ortoleva, J. Geophys. Res., [Solid Earth] **105**, 16 737 (2000).
[10] G. Daccord, Phys. Rev. Lett. **58**, 479 (1987).
[11] J. T. Wells, D. R. Janecky, and B. J. Travis, Physica D **47**, 115 (1991).
[12] D. R. Janecky *et al.*, in *Proceedings of 7th International Symposium on Water-Rock Interaction*, edited by Y. K. Kharaka and A. S. Maest (A. A. Balkema, Rotterdam, The Netherlands, 1992), p. 1043.
[13] P. B. Kelemen, J. A. Whitehead, E. Aharonov, and K. A. Jordahl, J. Geophys. Res., [Solid Earth] **100**, 475 (1995).
[14] S. Bekri, J. F. Thovert, and P. M. Adler, Chem. Eng. Sci. **50**, 2765 (1995).
[15] S. Bekri, J. F. Thovert, and P. M. Adler, Eng. Geol. (Amsterdam) **48**, 283 (1997).
[16] M. L. Hoefner and H. S. Fogler, AIChE J. **34**, 45 (1988).
[17] C. N. Fredd and H. S. Fogler, AIChE J. **44**, 1933 (1998).
[18] S. Chen and G. D. Doolen, Annu. Rev. Fluid Mech. **30**, 329 (1998).
[19] S. Succi, E. Foti, and F. Higuera, Europhys. Lett. **10**, 433 (1989).
[20] A. W. J. Heijs and C. P. Lowe, Phys. Rev. E **51**, 4346 (1995).
[21] A. K. Gunstensen and D. H. Rothman, J. Geophys. Res., [Solid Earth] **98**, 6431 (1993).

[22] D. Zhang, R. Zhang, S. Chen, and W. E. Soll, Geophys. Res. Lett. **27**, 1195 (2000).
[23] D. O. Martinez, W. H. Matthaeus, S. Chen, and D. C. Montgomery, Phys. Fluids **6**, 1285 (1994).
[24] A. K. Gunstensen, D. H. Rothman, S. Zaleski, and G. Zanetti, Phys. Rev. A **43**, 4320 (1991).
[25] X. Shan and H. Chen, Phys. Rev. E **47**, 1815 (1993).
[26] M. Swift, W. Osborn, and J. Yeomans, Phys. Rev. Lett. **75**, 830 (1995).
[27] X. He, R. Zhang, S. Chen, and G. D. Doolen, Phys. Fluids **11**, 1143 (1999).
[28] A. Ladd, Phys. Rev. Lett. **70**, 1339 (1993).
[29] F. Alexander, S. Chen, and J. Sterling, Phys. Rev. E **47**, R2249 (1993).
[30] Y. Qian, J. Sci. Comput. **8**, 231 (1993).
[31] X. He, S. Chen, and G. D. Doolen, J. Comput. Phys. **146**, 282 (1998).
[32] S. Chen, S. P. Dawson, G. D. Doolen, D. R. Janecky, and A. Lawniczak, Comput. Chem. Eng. **19**, 617 (1995).
[33] R. D. Kingdon and P. Schofield, J. Phys. A **25**, L907 (1992).
[34] S. P. Dawson, S. Chen, and G. D. Doolen, J. Chem. Phys. **98**, 1514 (1993).
[35] X. He, N. Li, and B. Goldstein, Mol. Simul. **25**, 145 (2000).